



JOINT INSTITUTE FOR NUCLEAR  
RESEARCH

Flevar Laboratory of Nuclear Reactions  
Chemistry of Transactinides

## **FINAL REPORT ON THE START PROGRAMME**

*Study of applications of photonuclear  
reactions at the MT-25 microtron*

**Supervisor:**

Dr. Nikolay V. Aksenov

**Student:**

Leira Liz Rodriguez Betancourt, Cuba  
University of Havana

**Participation period:**

September 08 – November 02,  
Summer Session 2024

Dubna, 2024

# Contents

<b>Abstract</b> .....	3
<b>Introduction</b> .....	4
<b>1.1. Environmental research</b> .....	5
<b>1.1.1. Brown coal</b> .....	5
<b>1.2. Production of medical radioisotopes</b> .....	6
<b>1.2.1. Platinum-195m</b> .....	6
<b>Project goals</b> .....	6
<b>Materials and Methods</b> .....	7
<b>2.1. Instrumental gamma activation analysis</b> .....	7
<b>2.2. Photonuclear reactions on <sup>nat</sup>Pt</b> .....	8
<b>Results and Discussion</b> .....	11
<b>3.1. Instrumental activation analysis</b> .....	11
<b>3.2. Photonuclear reactions on <sup>nat</sup>Pt</b> .....	13
<b>Conclusions</b> .....	17
<b>Acknowledgments</b> .....	17
<b>Referencias</b> .....	18

## **Abstract**

Photonuclear reactions play an important role in basic and applied nuclear physics research. In this work, photonuclear reactions have been initiated by bremsstrahlung. A rapid, non-destructive instrumental gamma activation analysis method for geochemical element analysis is introduced as a tool for the essential geochemical characterization of brown coal ashes. Also, the present study addressed the measurements of relative yields and cross section for photonuclear reactions on natural platinum using end-point energies of 10-23 MeV. Procedures were developed using a MT-25 microtron as a beam source and a High Purity Germanium (HPGe) gamma detector for measurements at Flevor Laboratory of Nuclear Reactions.

## Introduction

Photonuclear reactions play an important role in basic and applied nuclear physics research, they are defined as nuclear reactions induced by photons and occur when atomic nuclei are excited via the capture of incident photons and relax by emitting one or several elementary particles or nuclei fragments. At photon energies below 25-30 MeV, the excitation function of photonuclear reactions is characterized by a prominent peak, known as giant dipole resonance (GDR). This is a collective excitation of the atomic nucleus wherein nucleons move together, creating a large oscillation of the nucleus in the shape of a dipole. This energy range matches the upper limit of most electron accelerators, which produce "Bremsstrahlung" radiations. This process involves slowing down (or stopping completely, depending on the thickness of the target) the electrons in a target. The photon flux scales approximately quadratically with the target atomic number. Thus, high Z materials are typically selected as converter targets. The most commonly used are gold, tantalum or tungsten, although the use of lighter materials such as niobium and copper is also reported [1]. Electron bremsstrahlung produces a continuous spectrum of photons with the upper energy limit at the electron energy and the yield of photons increases as the energy decreases until, at low energies, self-absorption in the target reduces the yield. **Figure 1** shows the basic concept of achieving bremsstrahlung radiation.

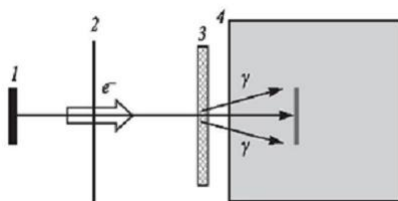


**Figure 1.** Simple geometry of target irradiation by bremsstrahlung. 1-electron source; 2-exit foil; 3-converter; 4-target.

Several facilities were constructed to investigate the fundamental aspects of the interaction of photons with matter. However, as research interests have evolved, many of these facilities have been shut down or been redirected to other research activities [2].

The Flevor Laboratory of Nuclear Reactions (FLNR) count with a compact electron accelerator- MT-25 microtron, shown in **Figure 2**. This equipment provides electron beam energies between 10 to 23 MeV with currents up to 20  $\mu\text{A}$  and have been attracted the attention of scientists, since is the simplest accessible source of radiation for investigation of  $(\gamma, n)$ ,  $(\gamma, a)$ ,  $(\gamma, p)$ ,  $(\gamma, f)$ ,  $(e, \gamma)$ ,  $(e, f)$ ,  $(\gamma, \gamma')$  and other photonuclear reactions and for development and application of nuclear-physical methods of elemental analysis [3] [4].

Microtron serves as a rather intensive source of both gamma rays and neutrons, which have been used for several studies involving activation analysis, photonuclear cross section measurements, and fundamental research using high-resolution gamma spectrometry.



**Figure 2.** Outlook of the MT-25 microtron in JINR, Dubna.

(<http://flevorlab.jinr.ru/mt-25-microtron/>)

### **1.1. Environmental research**

The activation methods are usually considered non-destructives in their instrumental modes and, in general, are employed for multi-elemental assay of samples of coal, rocks, minerals, plants, biological and other environmental matrices. In geochemical analysis, GAA (known also as gamma activation analysis) represents an advantageous alternative due to its lower sensitivity, lower activation cross sections and limited fluence rates in available irradiation facilities, allowing for the analysis of larger and more representative samples [5].

The use of microtron permits to determine in the instrumental version more than 40 elements, mainly by GAA, including trace elements interesting for geochemistry, industry and ecology, such as Cr, Ni, Zn, As, Rb, Sr, Y, Zr, Nb, Ag, Cd, Sn, I, Cs, Au, Hg, Tl, Pb, Th and U, with the detection limit  $10^{-3}$ - $10^{-5}$  % [4].

#### **1.1.1. Brown coal**

Besides carbon and organic matter, coal contains many elements, including the naturally occurring radionuclides of the U- and Th- series and the long-lived  $^{40}\text{K}$ . Moreover, brown coals are much more enriched with uranium and thorium than the hard ones. Brown coal is a medium-quality fuel used by thermal power plants, easy to burn due to its high volatile content. These elements associated with coal are mobilized during combustion and released as ashes or volatile compounds. Although their presence is usually at a trace level, the enormous quantities of coal used for producing electric energy make this one the most important source of emissions of trace elements to the environment and become a hazard for the human health [6].

This fact, together with a greater environmental awareness, have led to the realization of studies that attempt to characterize the possible impact of conventional thermal power plants on the environment. In this way, the interest

in this practice was centred on analyzing the metal content in ash samples from brown coal that thermal power plants in Mongolia would use.

## 1.2. Production of medical radioisotopes

In the last decade, the possibility of using photonuclear reactions to produce radionuclides for nuclear medicine has been established [1]. The production of radionuclides with an accelerator demands that particle beams be delivered with two specific characteristics. The beam must have sufficient energy to bring about the required nuclear reactions, and sufficient beam current to give practical yields. The FLNR MT-25 microtron meets these characteristics and has been established as an important installation for the production of wide variety of man-made radioactive isotopes.

### 1.2.1. Platinum-195m

Platinum is considered a noble metal, due to its relatively high chemical inertness. It is one of the rarest metals on the planet, yet one with a wide array of applications in science and industry [7]. Natural occurring platinum comprises six stable isotopes  $^{192}\text{Pt}$ ,  $^{194}\text{Pt}$ ,  $^{195}\text{Pt}$ ,  $^{196}\text{Pt}$ ,  $^{198}\text{Pt}$  and one long-lived radioisotope  $^{190}\text{Pt}$ . The isotope with the highest natural abundance is isotope  $^{195}\text{Pt}$ , which makes out 33.8 % of natural occurring platinum. This isotope is of great interest because it can be artificially transformed into the  $^{195\text{m}}\text{Pt}$  nuclear isomer, which undergoes an internal conversion process. As a result, emits a high number of Auger electrons (33 electrons per decay) making this radioisotope a suitable candidate for theranostics [8].

Many different nuclear reactions and pathways that can be used to make  $^{195\text{m}}\text{Pt}$ . Still, conventional methods are currently unable to provide enough specific activity to meet demands for radionuclide therapy, so it is relevant to continue research on  $^{195\text{m}}\text{Pt}$  production possibilities. A novel promising method to resolve the situation consist in the implementation of a photonuclear reactions based on natural platinum irradiation, using the brehmsstrahlung radiation.

Acurrate knowledge of interaction cross sections is crucial for scalable production of medical radionuclides, and the experimental data on the cross sections of photonuclear reactions on platinum isotopes are not available in the literature. Thus, to obtain more information regarding reactions with a higher degree of complexity, this study investigated photonucleon emission reactions on natural platinum target nuclei, expressed as  $^{\text{nat}}\text{Pt}(\gamma, n)$  and  $^{\text{nat}}\text{Pt}(\gamma, p)$  using bremsstrahlung end-point energies of 10-23 MeV.

### Project goals

The main purpose of the project is to make known the potential application of photonuclear reactions in the production of radiopharmaceutical agents and environmental research.

The main objetives of the study are:

1. Introduction to gamma activation analysis using MT-25 microtron through brown coal ash samples analysis.

2. Study of the reaction cross sections and relative yields for radiopharmaceutical grade quality  $^{195m}\text{Pt}$  production.
3. Analysis and interpretation of experimental results.

## Materials and Methods

### 2.1. Instrumental gamma activation analysis

In this study brown coal ash samples, obtained in laboratory condition at 650 °C, from brown coal of three different coal mines in Mongolia were analyzed. Each sample and geological reference material were placed in the cassettes organized forming a package, **Figure 3**, and were analyzed for definition of different elements contents. The reference material selected to represent brown coal ash was CGL-208-2. **Table 1** shows the details for the three samples we selected as an example for the measurement. The samples to analyze were collocated 5 cm from the source and irradiated, first on one side and then on the other, by the 23 MeV bremsstrahlung (the average electron current was 9.3-9.5  $\mu\text{A}$ ) for 2 h in total, on the MT-25 microtron. Irradiated samples were measured using the HPGe detector Canberra with FWHM resolution 1.5 keV and efficiency of 1% for the 1332.5 keV photons of  $^{60}\text{Co}$  (energy range to 3000 keV). Measurement times were 300, 900 and 3600 s for each sample and 100 s for copper coins. Spectrum processing was carried out by GENIE-2000 software.

**Table 1.** Brown coal ash samples data.

<i>Deposit</i>	<i>Coordinates*</i>			<i>Sample name</i>	<i>Mass (g)</i>
	<i>x</i>	<i>y</i>	<i>z</i>		
Bayanbogd	474013.9	4881563.5	-	Ash-1	2.7549
Shivee ovoo	5121856.867	310511.862	1084.026	Ash-15	1.5731
Baganuur	297843	5291866	-	Ash-21	2.5667

\* The coordinates shown are from the coal samples from which the ashes to be analyzed were obtained.

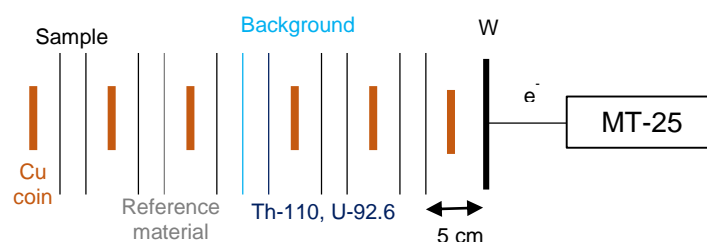


**Figure 3.** Experiment arrangement.

## 2.2. Photonuclear reactions on $^{nat}\text{Pt}$

This work was performed with the output electron beam of the MT-25 microtron. The electron energies were in the range of 10-23 MeV with an energy step of 1 MeV, the scheme of the experiments is shown in **Figure 4**. To produce gamma radiation, a radiator target made of tungsten was used. The tungsten target was sufficiently thick (3 mm) to maximize the number of photons in the energy range of the GDR that dominates the photonuclear cross section from the nucleon separation threshold to 25-30 MeV. To remove the remaining electrons from the bremsstrahlung beam, a 30 mm thick aluminum absorber was placed behind the tungsten converter. In order to determine the exact value of the current we used Cu foils with the same area of the Pt sample. For this purpose, targets were prepared making an assembly placing natural platinum and copper foils in a plastic round holder and have been irradiated. Irradiation times were chosen based on the predicted activity.

The changes in beam current were measured using a calibrated ionization chamber in the beam and a Faraday cup and recorded in a web-accessible database for use during the analysis employing an analog to digital converter card and LabView software. In addition to the ionization chamber and Faraday cup, the electrical charge collected on the target was digitalized and used to measure the beam current. The main parameters of the experiment are listed in **Table 2**.

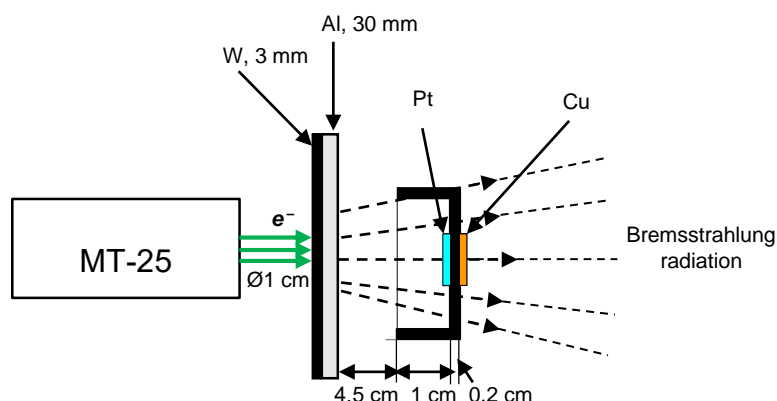


**Figure 4.** Irradiation scheme.

After irradiation, targets were consequently measured using a high purity germanium HPGe gamma detector with resolution of 16 keV at 1332 keV in combination with standard measurement electronics and a 16 K ADC/MCA (Multiport II Multichannel Analyzer, CANBERRA). The energy and efficiency calibrations of the HPGe detector were carried out using standard gamma-ray sources. The time from the end of irradiation to the start of measurement (cooling time) was in range from 10-15 min. For each sample, the spectra were measured at several times. Typical  $\gamma$ -ray spectra of the reaction products produced from  $^{nat}\text{Pt}$  are shown in **Figure 5**.



**Table 2.** Main parameters of the experiment.

<i>Electron energy (MeV)</i>	<i>Integral charge (mC)</i>	<i>Mass of platinum target (mg)</i>
23	5	40
22	5	80
21	5	80
20	5	80
19	5	800
18	5	800
17	5	800
16	10	800
15	30	800
14	30	800
13	50	800
12	50	800
11	50	800
10	50	800

The gamma-ray spectra were processed using the DEIMOS32 code [9], which fits the count area of the full-energy peaks with the Gaussian function. The identification of the processed peaks was based on the gamma-ray energy and intensity and the half-life of the generated residual nuclei. The radionuclides produced were identified based on their characteristic  $\gamma$ -ray energies and half-lives. The main  $\gamma$ -ray energies and intensities used to determine the yield of the reaction products are listed in **Table 3**.

**Table 3.** Spectroscopic data for the product nuclei from the photonuclear reactions on the stable isotopes of platinum. Columns 4 and 5 (\*) taken from [10].

Reaction product	Reactions	$E_{th}$ , MeV	$\gamma$ -ray energy, $E_\gamma$ /keV ( $I_\gamma$ / %)*	Half-life, $T_{1/2}$ *
$^{189}\text{Pt}$	$^{190}\text{Pt}(\gamma, n)^{189}\text{Pt}$	8.91	94.33 (7.6), 243.37 (7.0), 568.84 (7.1), 721.41 (9.3)	10.87 h
$^{191}\text{Pt}$	$^{192}\text{Pt}(\gamma, n)^{191}\text{Pt}$	8.67	82.41 (4.9), 359.9 (6), 409.44 (8), 538.90 (13.7)	2.83 d
$^{193m}\text{Pt}$	$^{194}\text{Pt}(\gamma, n)^{193m}\text{Pt}$	8.36	135.5 (0.112)	4.33 d
$^{195m}\text{Pt}$	$^{196}\text{Pt}(\gamma, n)^{195m}\text{Pt}$	7.92	98.857 (11.7), 129.7 (2.83)	4.01 d
$^{197g}\text{Pt}$	$^{198}\text{Pt}(\gamma, n)^{197g}\text{Pt}$	7.55	77.351 (17), 191.44 (3.7)	19.89 h
$^{197m}\text{Pt}$	$^{198}\text{Pt}(\gamma, n)^{197m}\text{Pt}$	7.55	53.10 (1.09), 279.01 (2.4), 346.5 (11.1)	95.41 min
$^{194g}\text{Ir}$	$^{195}\text{Pt}(\gamma, p)^{194g}\text{Ir}$	7.55	293.54 (2.52), 328.45 (13.1), 645.16 (1.18)	19.18 h
$^{195g}\text{Ir}$	$^{196}\text{Pt}(\gamma, p)^{195g}\text{Ir}$	8.25	129.7 (1.2), 211.41 (2.4)	2.29 h
$^{195m}\text{Ir}$	$^{196}\text{Pt}(\gamma, p)^{195m}\text{Ir}$	8.25	319.90 (9.4), 364.94 (9.3), 432.86 (9), 684.88 (9.4)	3.67 h

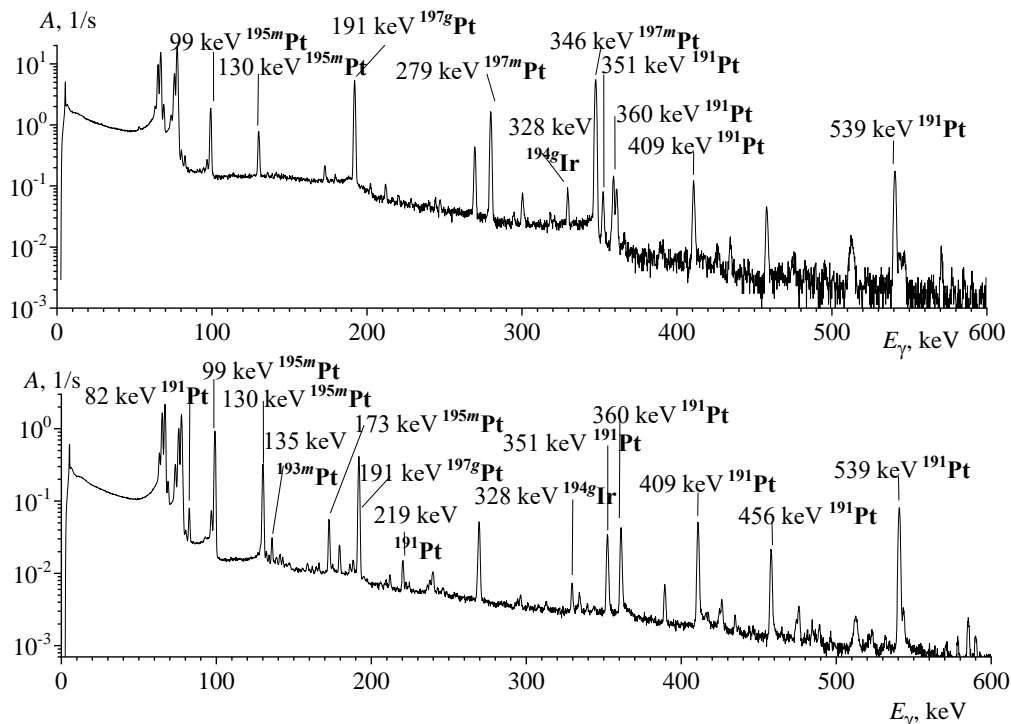


**Figure 5.** Spectra of residual activity of the irradiated sample of  $^{nat}\text{Pt}$  (top-to-bottom) 4 h (a) and 6 days (b) after irradiation. The spectra measurement duration was 1 h (a) and 1 day (b), respectively. The bremsstrahlung end-point energy used for the irradiation was 23 MeV.

## Results and Discussion

### 3.1. Instrumental activation analysis

In order to determine the exact value of the current, we used Cu coins, and the flow value calculated for those coins to correct the flow on the samples. **Figure 6** shows the correction for flow value in % for each sample and Cu monitors. Measurements were carried out at three different times after irradiation for each samples, 1h for detecting short half-life elements, 1 day for detecting medium half-life elements and 10 days for detecting long half-life elements. **Table 4** shows the chemical elements can be analyzed using the electron accelerator MT-25 microtron and **Figure 7** shows the chemical elements detected during the measurements of the sample Ash-1, elements were identified using elements main lines. For the determination of the chemical elements concentration in our samples, also calculated cooling time for each measurement.

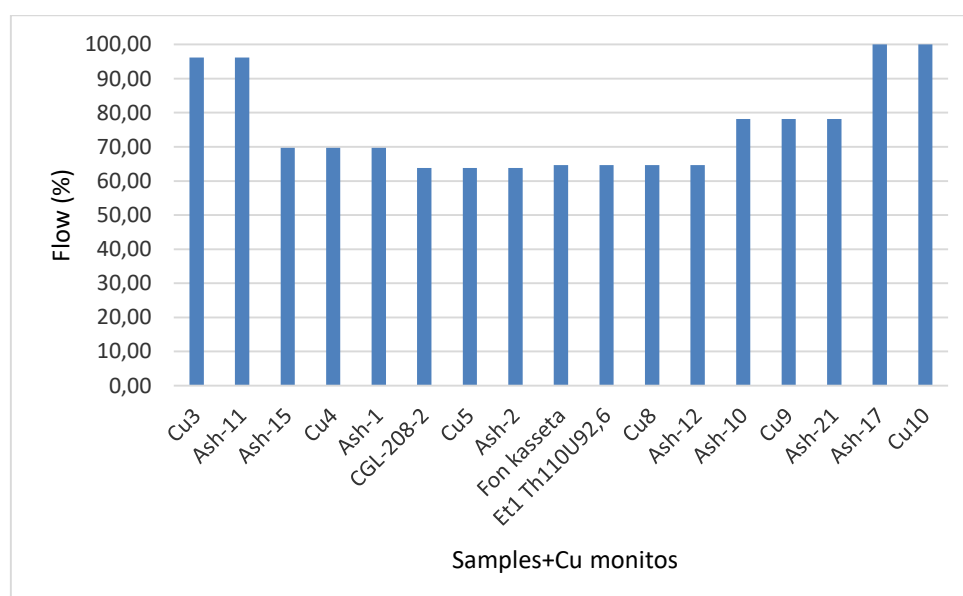


**Figure 6.** Flow in percent for each sample and Cu monitors.

The results of measuring metal concentration in the samples of brown coal ash are shown in **Table 5**.

During coal combustion, uranium and thorium are concentrated in the ash slag. It was found that uranium concentrations in samples Ash-1 and Ash-15 are less than global average value for ashes of brown coals. In contrast, sample Ash-21 presented approximately double the concentration average value. Thorium was found in concentrations approximately 1.5 more than the Clarke value.

**Table 4.** The chemical elements analyzed using the electron acelerator MT-25 microtron. The detection limit is given in g/g ( $^{232}\text{Th}$ ,  $^{238}\text{U}$ ,  $^{237}\text{Np}$  and  $^{239}\text{Pu}$  in g).

H																	He
$1\cdot 10^{-4}$																	
Li	Be	B	C	N	O	F								Ne			
$3\cdot 10^{-7}$	$1\cdot 10^{-6}$	$3\cdot 10^{-7}$		$1\cdot 10^{-7}$	$1\cdot 10^{-6}$												
Na	Mg	Al	Si	P	S	Cl								Ar			
$2\cdot 10^{-4}$	$2\cdot 10^{-4}$	$2\cdot 10^{-5}$	$1\cdot 10^{-3}$			$1\cdot 10^{-6}$											
K	Ca	Sc	Ti	V	Cr	Mn	Fe	Co	Ni								
$2\cdot 10^{-4}$	$2\cdot 10^{-4}$	$8\cdot 10^{-7}$	$1\cdot 10^{-4}$	$5\cdot 10^{-6}$	$5\cdot 10^{-6}$	$4\cdot 10^{-7}$	$1\cdot 10^{-3}$	$1\cdot 10^{-6}$	$1\cdot 10^{-6}$								
Cu	Zn	Ga	Ge	As	Se	Br	Kr										
$1\cdot 10^{-5}$	$5\cdot 10^{-6}$	$1\cdot 10^{-5}$	$1\cdot 10^{-5}$	$5\cdot 10^{-7}$	$1\cdot 10^{-5}$	$5\cdot 10^{-6}$											
Rb	Sr	Y	Zr	Nb	Mo	Tc	Ru	Rh	Pd								
$2\cdot 10^{-6}$	$2\cdot 10^{-7}$	$2\cdot 10^{-6}$	$6\cdot 10^{-7}$	$1\cdot 10^{-6}$	$1\cdot 10^{-6}$		$1\cdot 10^{-5}$	$1\cdot 10^{-4}$	$4\cdot 10^{-7*}$								
Ag	Cd	In	Sn	Sb	Te	I	Xe										
$1\cdot 10^{-6}$	$5\cdot 10^{-6}$	$1\cdot 10^{-7}$	$1\cdot 10^{-5}$	$5\cdot 10^{-7}$	$1\cdot 10^{-6}$	$3\cdot 10^{-6}$											
Cs	Ba	La	Hf	Ta	W	Re	Os	Ir	Pt								
$5\cdot 10^{-7}$	$5\cdot 10^{-6}$			$5\cdot 10^{-8}$	$1\cdot 10^{-7}$	$7\cdot 10^{-7}$	$1\cdot 10^{-4}$	$1\cdot 10^{-5}$	$1\cdot 10^{-7*}$								
Au	Hg	Tl	Pb	Bi	Po	At	Rn										
$2\cdot 10^{-8}$	$5\cdot 10^{-7}$	$7\cdot 10^{-7}$	$2\cdot 10^{-6}$														
Fr	Ra	Ac	Rf	Db	Sg	Bh	Hs	Mt	110								
Ce	Pr	Nd	Pm	Sm	Eu	Gd	Tb	Dy	Ho	Er	Tm	Yb	Lu				
$1\cdot 10^{-6}$		$2\cdot 10^{-6}$		$5\cdot 10^{-8}$	$1\cdot 10^{-7}$					$1\cdot 10^{-7}$							
Th	Pa	U	Np	Pu	Am	Cm	Bk	Cf	Es	Fm	Md	No	Lr				
$5\cdot 10^{-8}$		$5\cdot 10^{-8}$	$3\cdot 10^{-14*}$	$2\cdot 10^{-14*}$	$5\cdot 10^{-14*}$												
$1\cdot 10^{-13*}$		$5\cdot 10^{-14*}$		$3\cdot 10^{-14*}$													
		$4\cdot 10^{-14*}$															

E  
( $\gamma$ , n; n,  $\gamma$ )  
( $\gamma$ , f)/(n, f)

\*radiochemical method

**Table 5.** Elements concentration in the samples of brown coal ash. \*Values converted to % from [11]

Elements	Elements concentration (%)			World coal ash (%)*
	Ash-1	Ash-15	Ash-21	
Na	1.88±0.03	0.60±0.03	0.15±0.01	-
Mg	3.011±0.012	2.637±0.015	0.818±0.006	-
Ca	5.78±0.07	15.32±0.13	4.73±0.06	-
Sc	0.0019±0.0002	0.0006±0.0002	0.0014±0.0001	0.0023±0.0001
Ti	0.35±0.03	0.28±0.03	0.30±0.02	0.40±0.02
Ni	0.0061±0.0003	0.0017±0.0003	0.0037±0.0002	0.0052±0.0005
As	0.0174±0.0002	0.0010±0.0001	0.0053±0.0001	0.0048±0.0007
Sr	0.0702±0.0003	0.1864±0.0008	0.0456±0.0003	0.074±0.007
Th	0.0030±0.0001	0.0028±0.0004	0.0027±0.0001	0.0019±0.0001
U	0.00059±0.00006	0.00119±0.00007	0.00323±0.00006	0.0016±0.0002

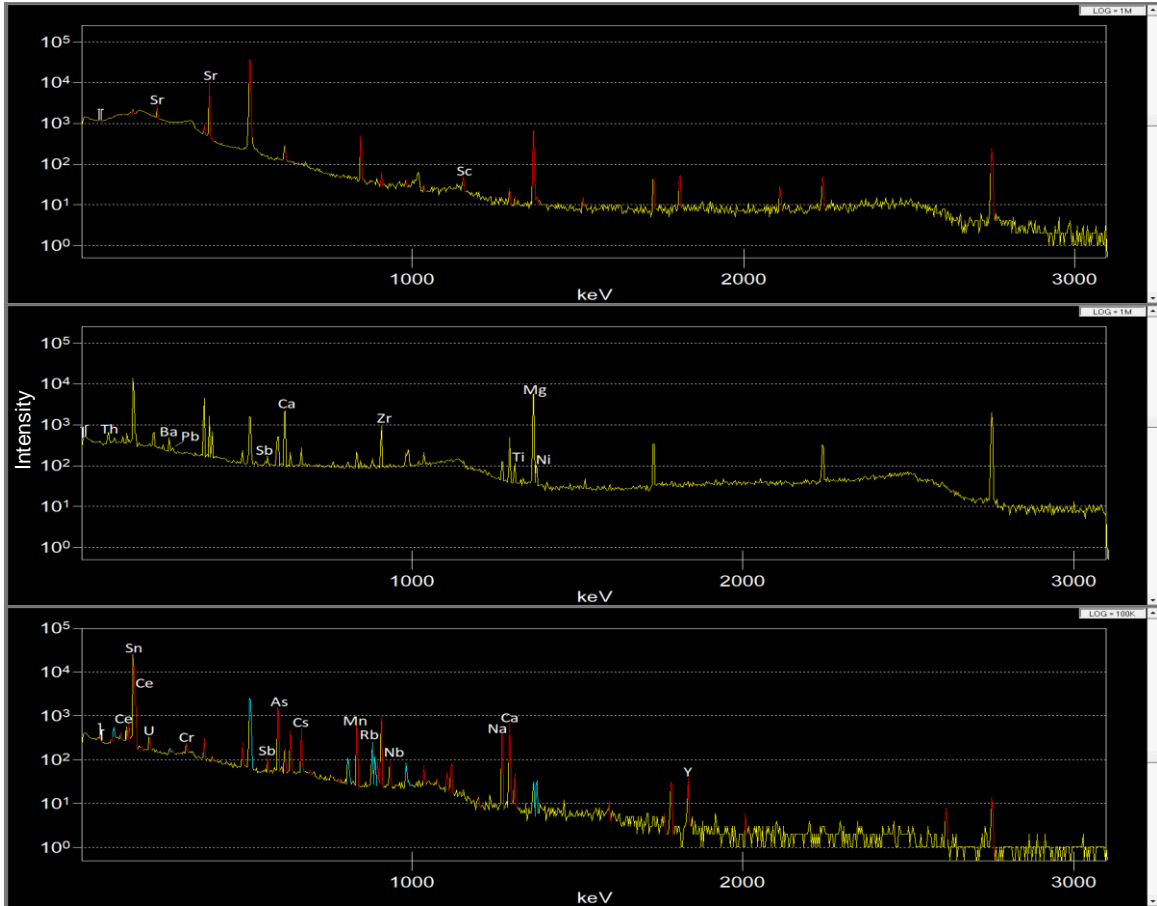


**Figure 7.** Spectra of sample Ash-1 after irradiation (top to bottom) 1h (a), 1d (b) and 10 d (c). Only are shown the main lines of each chemical element that can be identified in first, second and third measurement respectively.

### 3.2. Photonuclear reactions on $^{nat}\text{Pt}$

The experimental yields of the reactions  $Y_{exp}$  were normalized to one electron of the accelerated beam incident on the bremsstrahlung target and calculated using the following formula:

$$Y_{exp} = \frac{S_p \cdot C_{abs}}{\epsilon \cdot I_\gamma} \frac{t_{real}}{t_{live}} \frac{1}{N} \frac{1}{N_e} \frac{e^{\lambda \cdot t_{cool}}}{(1 - e^{-\lambda \cdot t_{real}})} \frac{\lambda \cdot t_{irr}}{(1 - e^{-\lambda \cdot t_{irr}})} \quad (1)$$

where  $S_p$  is the full-energy-peak area;  $\epsilon$  is the full-energy-peak detector efficiency;  $I_\gamma$  is the gamma emission probability;  $\cdot C_{abs}$  is the correction for self-absorption of gamma rays in the sample;  $t_{real}$  and  $t_{live}$  are the real time and live time of the measurement, respectively;  $N$  is the number of atoms in the activation sample;  $N_e$  is the integral number of incident electrons;  $\lambda$  is the decay constant;  $t_{cool}$  is the cooling time; and  $t_{irr}$  is the irradiation time.

The main disadvantage of bremsstrahlung beam experiments is that the yield of photonuclear reaction depends both on the studied cross section of the reaction  $\sigma(E)$  and the shape of the bremsstrahlung spectrum  $W(E, E_{\gamma max})$ , which is often known with insufficient accuracy. That is the reason why the data obtained from

photonuclear experiments on bremsstrahlung beams are generally represented in terms of the relative yields or the integrated reaction cross section, flux weighted average cross section  $\langle\sigma\rangle$ , or cross section per equivalent photon  $\sigma_q$  [9].

The use of the relative yields makes it possible to obtain the dependence of the probability of photonuclear reactions on the maximum energy of bremsstrahlung under different experimental conditions. The calibration with respect to the yield of the most probable reaction excludes the influence of the total photon absorption cross section. In our case, the dominant reaction is  $^{198}\text{Pt}(\gamma, n)^{197\text{m}}\text{Pt}$ . Theoretical values of the relative yields can be calculated using the following formula:

$$Y_{rel,i} = \frac{\sum_i \eta_i \int_{E_{th}}^{E_{\gamma max}} \sigma_i(E) W(E, E_{\gamma max}) dE}{\eta_{Pt-198} \int_{E_{th}}^{E_{\gamma max}} \sigma_{(\gamma,n)}(E) W(E, E_{\gamma max}) dE} \quad (2)$$

While, flux weighted average cross section and cross section per equivalent photon can be calculated using the 3 and 4 formulas respectively:

$$\langle\sigma\rangle = \frac{\int_{E_{th}}^{E_{\gamma max}} \sigma(E) W(E, E_{\gamma max}) dE}{\int_{E_{th}}^{E_{\gamma max}} W(E, E_{\gamma max}) dE} \quad (3)$$

$$\sigma_q = \frac{\eta \int_{E_{th}}^{E_{\gamma max}} \sigma(E) W(E, E_{\gamma max}) dE}{\frac{1}{E_{\gamma max}} \int_0^{E_{\gamma max}} E \cdot W(E, E_{\gamma max}) dE} \quad (4)$$

**Figure 8** shows experimental value of the relative yield of photoneutron reaction  $^{198}\text{Pt}(\gamma, n)^{197\text{m}}\text{Pt}$  normalized to the yield of the reaction  $^{198}\text{Pt}(\gamma, n)^{197\text{m}}\text{Pt}$  (**Table 6** contains exactly this for different photonuclear reactions). Within the limits of error our result on relative yields of the  $^{190,192,194,196,198}\text{Pt}(\gamma, n)$  reactions agrees well with calculation based on TALYS code. In the case of  $^{195,196}\text{Pt}(\gamma, p)$  reactions, experimental results are much larger than the TALYS theoretical calculations.

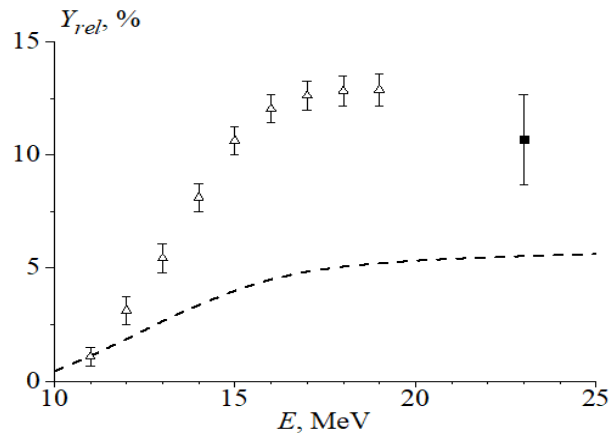


**Figure 8.** Relative yield of  $^{198}\text{Pt}(\gamma, n)^{197\text{m}}\text{Pt}$  reaction as a function of bremsstrahlung end-point energy from the present work (solid rectangle) and simulated values using TALYS code (dashed lines) base on monoenergetic photons.

**Table 6.** Relative yields for the photonuclear reactions on stable isotopes of  $^{nat}\text{Pt}$ .

Reactions	Relative yields, %		Exp / TALYS
	Experiment	TALYS	
$^{190}\text{Pt}(\gamma, n)^{189}\text{Pt}$	$0.15 \pm 0.03$	0.14	1.1
$^{192}\text{Pt}(\gamma, n)^{191}\text{Pt}$	$8.14 \pm 1.56$	9.66	0.9
$^{194}\text{Pt}(\gamma, n)^{193m}\text{Pt}$	$51 \pm 9$	37	1.5
$^{196}\text{Pt}(\gamma, n)^{195m}\text{Pt}$	$33 \pm 6$	27	1.3
$^{198}\text{Pt}(\gamma, n)^{197g}\text{Pt}$	$89 \pm 21$	94	1.0
$^{198}\text{Pt}(\gamma, n)^{197m}\text{Pt}$	$11 \pm 2$	6	2.1
$^{195}\text{Pt}(\gamma, p)^{194g}\text{Ir}$	$0.5 \pm 0.1$	0.04	13
$^{196}\text{Pt}(\gamma, p)^{195g}\text{Ir}$	$0.25 \pm 0.05$	0.02	13
$^{196}\text{Pt}(\gamma, p)^{195m}\text{Ir}$	$0.33 \pm 0.07$	0.001	330

**Figure 9** shows flux weighted average cross section and cross section per equivalent photon of photoneutron reactions  $^{198}\text{Pt}(\gamma, n)^{197m}\text{Pt}$  and  $^{198}\text{Pt}(\gamma, n)^{197m+g}\text{Pt}$  (**Table 7** contains exactly this for different photonuclear reactions).

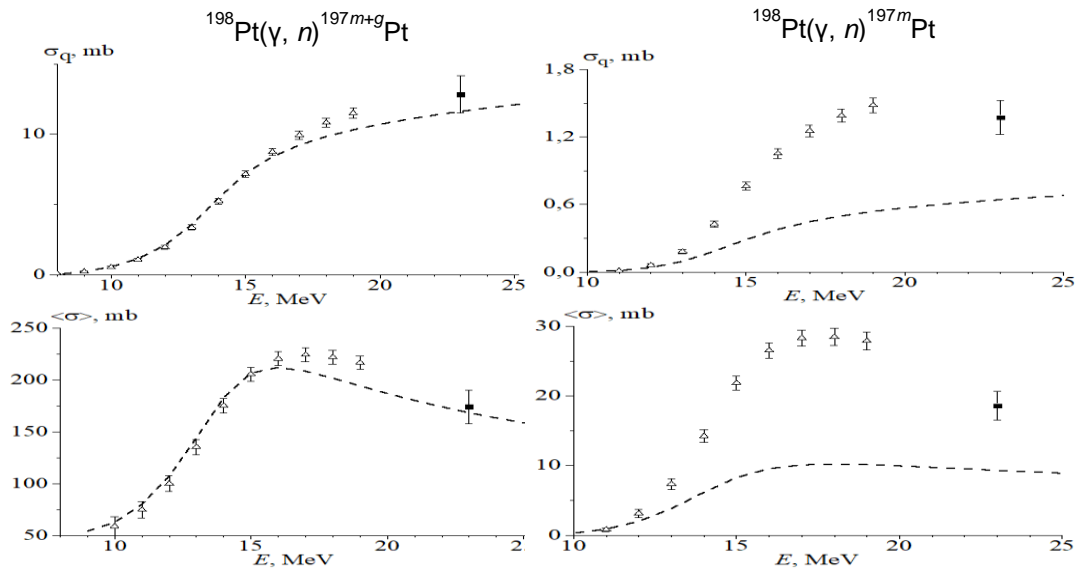


**Figure 9.** flux weighted average cross section and cross section per equivalent photon of photoneutron reactions  $^{198}\text{Pt}(\gamma, n)^{197m}\text{Pt}$  and  $^{198}\text{Pt}(\gamma, n)^{197m+g}\text{Pt}$ .

**Table 7.** Cross sections per equivalent quantum and flux-averaged cross sections for the photonuclear reactions on stable isotopes of <sup>nat</sup>Pt.

Reactions	$\sigma_q$ , mb	$\langle\sigma\rangle$ , mb
<sup>190</sup> Pt( $\gamma$ , $n$ ) <sup>189</sup> Pt	0.019 ± 0.002	202 ± 24
<sup>192</sup> Pt( $\gamma$ , $n$ ) <sup>191</sup> Pt	1.04 ± 0.12	165 ± 19
<sup>194</sup> Pt( $\gamma$ , $n$ ) <sup>193m</sup> Pt	6.6 ± 0.8	25 ± 3
<sup>196</sup> Pt( $\gamma$ , $n$ ) <sup>195m</sup> Pt	4.2 ± 0.5	20 ± 2
<sup>198</sup> Pt( $\gamma$ , $n$ ) <sup>197g</sup> Pt	11.5 ± 2.1	155 ± 26
<sup>198</sup> Pt( $\gamma$ , $n$ ) <sup>197m</sup> Pt	1.37 ± 0.15	18 ± 2
<sup>195</sup> Pt( $\gamma$ , $p$ ) <sup>194g</sup> Ir	0.070 ± 0.008	0.70 ± 0.08
<sup>196</sup> Pt( $\gamma$ , $p$ ) <sup>195g</sup> Ir	0.032 ± 0.005	0.54 ± 0.08
<sup>196</sup> Pt( $\gamma$ , $p$ ) <sup>195m</sup> Ir	0.042 ± 0.007	0.71 ± 0.12



## **Conclusions**

The potential application of photonuclear reactions as a new route of production of medical radioisotopes and in environmental research was demonstrated through gamma activation analysis of brown coal ash samples and the study of cross section and relative yields of reactions on natural platinum. The brown coal ash samples were irradiated by the 23 MeV bremsstrahlung. Different chemical elements were detected during the measurements and were identified using elements main lines. The concentrations in % of a group of the elements detected in three of the samples were calculated. It was found that uranium concentrations in samples Ash-1 and Ash-15 are less than global average value for ashes of brown coals, while sample Ash-21 presented approximately double the concentration average value. Thorium was found in concentrations approximately 1.5 more than the Clarke value.

Photonuclear reactions on natural platinum were carried out using bremsstrahlung end-point energies of 10-23 MeV. The experimental results were compared with calculations using TALYS model with the standard parameters. For the obtained photoneutron reactions, within the limits of error, a good agreement was observed between the experimental relative yields and calculations according to the TALYS program. For the photoproton reactions experimental results are much larger than the TALYS theoretical calculations. The study of photonuclear reactions on platinum isotopes is important for understanding the formation and decay of nuclei during nucleosynthesis.

## **Acknowledgments**

I would like to thank the JINR team and the START Program for the opportunity and support, as well my supervisor, Dr. Nikolay V. Aksenov, the staff of Sector N3 of the Flevor Laboratory of Nuclear Reactions and their collaborators for their guidance, advice and cooperation on the course of this project.

## Referencias

- [1] S. Braccini, P. Casolaro, P. Casolaro, C. Kottler, M. Lüthi, L. Mercolli, P. Peier, P. Scampoli y A. Türler, «Methodology for measuring photonuclear reaction cross sections with an electron accelerator based on Bayesian analysis,» *Applied radiation and isotopes*, vol. 208, p. 111275, 2024.
- [2] I. A. E. Agency, Photonuclear production of radioisotopes, Vol. IAEA-TECDOC-2051, Viena: International Atomic Energy Agency, 2024.
- [3] O. Maslov, A. Belov, G. Y. Starodub y S. Dmitriev, «Activation analysis of environmental samples using the MT-25 microtron of the FLNR,» *Analytical Science and Technology*, vol. 8, pp. 815-820, 1995.
- [4] O. Maslov y S. Dmitriev, «Use of MT-25 microtron for scientific and applied investigations,» 2003.
- [5] I. Krausová, J. Mizera, Z. Řanda, D. Chvátíl y P. Krist, «Instrumental Photon Activation Analysis with Short-Time Irradiation for Geochemical Research,» *Minerals*, vol. 11, p. 617, 2021.
- [6] N. Gustova, S. Kaplina, M. Gustova y N. Baljinnyam, «The Study of the Radioecological Situation in the Environment Surroundings the Coal Power Plant,» *Physics of Particles and Nuclei Letters*, vol. 19, pp. 298-301, 2022.
- [7] J. R. d. Laeter, J. K. Böhlke, P. D. Bièvre, H. Hidaka, H. S. Peiser y K. J., «Atomic weights of the elements. Review,» *Pure and Applied Chemistry*, vol. 75, pp. 683-800, 2003.
- [8] A. Madumarov, N. Aksenov y G. Bozhikov, «Consideration of reactor and photonuclear pathways to produce <sup>195m</sup>Pt for theranostics applications,» de *NINTH INTERNATIONAL CONFERENCE ON RADIATION IN VARIOUS FIELDS OF RESEARCH (RAD 2021)*, Montenegro, 2021.
- [9] F. Rasulova, N. Aksenov, S. Alekseev, R. Aliev, S. Belyshev, I. Chuprakov, N. Fursova, A. Madumarov, J. Khushvaktov, A. Kuznetsov y B. Yuldashev, «Photonuclear reactions on stable isotopes of selenium at bremsstrahlung,» *Chinese Physics C*, vol. 48, 2024.
- [10] B. N. L. National Nuclear Data Center, «Nudat3,» [En línea]. Available: <http://www.nndc.bnl.gov/nudat3>.
- [11] M. Ketris y Y. and Yudovich, «Estimations of Clarkes for Carbonaceous biolithes: World averages for trace elements contents in black shales and coals,» *International Journal of Coal Geology*, vol. 78, pp. 135-148, 2009.